IEEE Access
Multidisciplinary | Rapid Review | Open Access Journal

Received June 20, 2018, accepted July 24, 2018, date of publication August 2, 2018, date of current version August 28, 2018.

Digital Object Identifier 10.1109/ACCESS.2018.2862427

A Method to Estimate Power System Voltage Stability Margins Using Time-Series From Dynamic Simulations With Sequential Load Perturbations

V. S. NARASIMHAM ARAVA[1], (Member, IEEE), AND LUIGI VANFRETTI[2], (Senior Member, IEEE)

[1]WAMS Center of Excellence, GE, Edinburgh EH3 5DA, U.K.
[2]Department of Electrical and Computer, Rensselaer Polytechnic Institute, Troy, NY 12180 USA

Corresponding author: V. S. Narasimham Arava (narasimham.arava@ge.com)

The work of V. S. Narasimham Arava was supported by the European Union Seventh Framework Programme (FP7/2007-2013) under Grant 283012, within Innovative Tools for Electrical System Security within Large Areas (iTESLA). The work of L. Vanfretti was supported in part by the European Union Seventh Framework Programme (FP7/2007-2013) under Grant 283012, within Innovative Tools for Electrical System Security within Large Areas (iTESLA), in part by the Engineering Research Center Program of the National Science Foundation and the Department of Energy under Award EEC-1041877, and in part by the CURENT Industry Partnership Program.

ABSTRACT In this paper, a methodology to assess power system voltage stability margins from time-series data is presented. The proposed method obtains time-series from dynamic simulations subject to sequential load changes that are then used as an input to a voltage stability estimation method. After a contingency is applied, load perturbations aim to move the system through different loading levels. This approach allows estimating voltage stability margins from time-series without any information or numerical quantities of the mathematical model of the system other than the simulation's output. This is useful for dynamic security assessment systems that only have transient simulators for their workflows and still require to estimate the voltage stability margins. The proposed method is used to quantify the severity of the contingencies using a three-layer index. The proposed approach is illustrated using a simple two-bus system and then tested using time-domain simulations of the Nordic-44 Bus test system.

INDEX TERMS Power systems, time-domain simulation, voltage stability.

I. INTRODUCTION

A. MOTIVATION

The challenge brought by the ongoing energy transition has lead electric utilities to operate closer to their operating-limits. Near real-time monitoring and operation tools can help to mitigate potential undesired behavior, by providing means to operate the system with more flexibility, adapt to intermittent generation sources [1], and in addition, to securely address the increase in the number of large-scale outages [2]. This paper describes a method that aids operational tools in determining voltage stability margins from time-series of dynamic simulators within a dynamic security assessment platform.

B. PREVIOUS WORK

The main categories of computations performed for voltage stability analysis purposes are contingency analysis and security margin calculations [3]. Contingency analysis methods determine system's response due to loss of N-1 critical components, at a given operating point. Static and dynamic time-domain simulation methods are generally used in contingency analysis to assess the voltage stability of a given power system [4]. Static methods focus on the existence of equilibria and therefore rely on the solution of non-linear algebraic equations that assume equilibrium conditions of the system's dynamics [5]. Power flow-based contingency analysis and continuation power flow (CPF) are some examples of static methods [6]. Static methods are usually very efficient but they neither account for post contingency control actions that depend on the system's evolution, nor do they capture more complex instability mechanisms. Time-domain methods, on the other hand, are generally computationally demanding, but offer higher accuracy and better information (e.g. w.r.t the system's response to a sequence of events) [3].

C. DYNAMIC SECURITY ASSESSMENT (DSA) TOOLS

The scope of the DSA is to provide Energy Management System (EMS) operators with a tool for transient/voltage/small-signal stability analysis to be used on-line during the normal cycle of real time operation and off-line with the purpose of analysis [7]–[10]. DSA tools can be integrated with EMS [11] and can be operated in two modes: (i) On-line mode: using the network data and State Estimation (SE) solutions, and (ii) Off-line mode: to execute offline analysis applications for operational planning. The firsthand experience and challenges of using the DSA tools by utilities is provided in [12] and [13]. To address some of the challenges, the FP7 iTesla[1] project aimed to build a software toolbox to, among many goals, provide the means to perform DSA [14]–[16]. To this end, the off-line analysis workflow within the iTesla toolbox performs a contingency impact assessment using time-domain simulations [17]. This impact assessment is performed by calculating pre-and-post-contingency severity indexes.

D. VOLTAGE STABILITY ASSESSMENT

Large efforts have been made to understand voltage stability better, to detect it faster, and to evolve a strategy to mitigate it once its likelihood is observed. To this purpose, it is essential to estimate the maximum permissible loading of a system using the information about the current operating point. The conventional PV or VQ curves are used as a tool for assessing voltage stability and to find the maximum loading at the verge of voltage collapse. These curves are generated by running many power flow cases using conventional methods. While such procedures can be automated, they are time-consuming and do not readily provide all information required to determine the causes of stability problems. To overcome these disadvantages several techniques have been proposed in the literature, such as bifurcation theory, energy methods, eigenvalue and singular value methods [18]–[20] etc. However, these methods are computationally intensive, which makes them less viable for fast computation during a sequence of discontinuities, e.g. generators violating field current or reactive limits etc. Moreover, in the present deregulated context, a quick computation is necessary to take adequate corrective actions in time to save the system from an impeding voltage collapse.

In this paper, the time-domain simulation method adopted for voltage stability analysis in the iTesla platform (https://github.com/itesla/ipst) is analyzed and expanded. This method requires time-series from dynamic simulations because of: (a) lack of access to the core of power flow tools to exploit the static model, (b) no availability of a CPF tool and, more importantly, (c) because of the aforementioned advantages. In the authors' previous work used in the iTesla platform, the original methodology required the execution of three dynamic simulations, at three different loading levels for a given network. While this approach provides good estimates of the margin, it also increases the computational requirements from $O(n)$ to $O(3n)$ (where n is the number of time-domain simulations to be executed). In order to reduce the computational burden and to keep adequate estimation accuracy, while at the same time comply with the single-simulation contingency workflow requirements of iTesla toolbox (which are similar to other DSA tools [20]), a new method is proposed here.

The benefit of the method is therefore to provide means to assess a large number of simulations by analyzing their time series, while at the same keeping computational requirements in the $O(n)$ order. The outputs of this method are to be used within the DSA tool to derive rules for operators, which can be built using decision trees [20].

E. CONTRIBUTION

This paper proposes a new method to calculate the severity index using a new method to estimate a Thevenin equivalent using a Total Least Squares (TLS) algorithm and offers the following contributions.

- The proposed method requires only one time-domain simulation per contingency, and the accuracy of the margin's estimation is maintained by introducing load perturbations to identify any slow-voltage dynamic characteristics of the system.
- The paper investigates the method's performance during pre- and post- contingency states and accuracy comparisons are made with the previous method.
- The value of the new method in synthesizing the information is highlighted by calculating a data synthesis factor that is compared with the previous method.
- Case studies are performed by simulating the dynamic response of a simple two-bus system and the Nordic 44 bus system [21], [22].

The remainder of this paper is organized as follows. Section II explains the equivalent model estimation along with the severity index computations. Section III describes the proposed methodology. Section IV illustrates the computational and accuracy analysis with the proposed method. Section V presents the results obtained when the proposed method is applied to the Nordic 44 bus system. Conclusions are drawn in Section VI.

II. EQUIVALENT MODEL ESTIMATION AND SEVERITY INDEX COMPUTATIONS

Voltage stability (VS) is the system's capability of keeping the voltages at buses close to their nominal values after a disturbance [2]. Voltage instability phenomena can be identified using both static and dynamic analysis methods. The approach proposed here is to identify equivalent power system models from the time series of dynamic simulations and use them to predict the voltage stability limit [23].

A. SINGLE VOLTAGE SOURCE AND LOAD MODEL

The Thevenin equivalent of the power system as viewed from a single measurement location neglecting losses is shown in Fig. 1. The equivalent model parameters (E, δ, X) are calculated from time series (V_i, P_i, Q_i) data as described in [23].

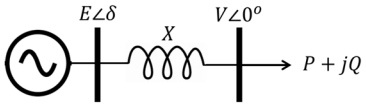

FIGURE 1. Equivalent model.

The method presented in [23] considered a linear P-Q load model as shown in (1).

$$Q = \alpha + \beta P \tag{1}$$

The values of α and β are calculated by solving a least square problem, as described in [23]. This linear P-Q load model can be combined with the single voltage source model in order to calculate the PV curve and the voltage stability limit for the power transfer at the bus of interest by solving (2).

$$P^2X^2 - E^2V^2 + (\alpha X + \beta PX + V^2)^2 = 0 \tag{2}$$

B. THREE LAYER SEVERITY INDEX

The three layers of the index are: Single Bus Index (SBI), All Buses Index (ABI) and Global Bus Index (GBI). The **SBI** is a $R^{(2Nb\times b)}$ matrix where Nb is the number of buses under analysis. The SBI provides the distance in pre-and-post contingency for the power (P_{lim}) and voltage (V_{lim}) limits of a selected bus or group of buses. The SBI is defined in [13] and is divided as follows: column 1-3 correspond to the distance from each of the given loading level to the limit with respect to power while column 4-6 corresponds to the distance for each loading level to the limit with respect to the voltage. In the SBI, for each bus, there are four rows, odd rows correspond to pre-contingency data and even rows correspond to post-contingency data. The SBI is mathematically given by, (3), as shown at the bottom of this page, where

$$sb_{(i,j)} = \frac{P_{i,\lim} - P_{i,j}}{P_{i,\lim}}, \quad sb_{(i,k)} = \frac{V_{i,\lim} - V_{i,k}}{V_{i,\lim}},$$
$$sb_{(i',j)} = \frac{P_{i',\lim} - P_{i',j}}{P_{i',\lim}}, \quad sb_{(i',k)} = \frac{V_{i',\lim} - V_{i',k}}{V_{i',\lim}},$$
$$sb_{(r,j)} = \frac{\hat{P}_{r,\lim} - \hat{P}_{r,j}}{\hat{P}_{r,\lim}}, \quad sb_{(r,k)} = \frac{\hat{V}_{r,\lim} - \hat{V}_{r,k}}{\hat{V}_{r,\lim}},$$

with $i = 1, 4, 7...n$; $i' = 1, 4, 7...n'$; $j = 1, 2, 3$; $r = 3, 6, 9$; $k = 4, 5, 6$; $m = 2Nb$; $n = m - 1$; $m' = 2Nb$; $n' = m' - 1$

If an element of the SBI is negative, then the power or the voltage at the same loading level has exceeded the operational limits. It should be noted that the voltage and power limits considered are not the theoretical maximum loadability limits but operational limits i.e. a ε smaller than the theoretical limits. ε is set to the best judgement of the analyst, e.g. $P_{\max} = P_{\max} - \varepsilon P_{\max}$.

The All Bus Index **ABI** is a $R^{(1\times 6)}$ vector with the loading points of the bus that has the minimum distance to the power and voltage limits in pre-and-post contingency and is defined as (4), as shown at the bottom of this page, where *i, j, r* and *k* are defined in (3).

The Global Bus Index **GBI** is a 2-element vector that provides the overall minimum distance to the power and voltage limits with respect to all the buses, thus synthesizing the ABI.

$$\begin{aligned} GBI &= \begin{bmatrix} \Delta\bar{P} & \Delta\bar{V} \end{bmatrix} \\ \Delta\bar{P} &= \min \begin{vmatrix} \Delta\hat{P}_{a(1,1)} & \Delta\hat{P}_{b(1,2)} & \Delta\hat{P}_{c(1,3)} \end{vmatrix}, \\ \Delta\bar{V} &= \min \begin{vmatrix} \Delta\hat{V}_{a(1,1)} & \Delta\hat{V}_{b(1,2)} & \Delta\hat{V}_{c(1,3)} \end{vmatrix} \end{aligned} \tag{5}$$

The values of SBI and consequently, ABI and GBI are computed from the above expressions.

The GBI allows to monitor if a contingency poses a voltage stability issue. Then ABI and SBI indexes can be used within the DSA tool to derive rules for operators, which can be built using decision trees [18]. Note that the variable εwill allow to provide an acceptable answer even though there might be uncertainties in both the model (and its parameters) and or the results of the simulation itself (time-series data). This can be considered as taking a ''safety margin'' from the maximum loadability point to deal with modeling uncertainties.

III. PROPOSED METHODOLOGY

A. NEED FOR A NEW METHODOLOGY

The approach presented in [24] provides a good estimate of the voltage stability margins. However, in order to reduce the

$$SBI = \begin{bmatrix} sb_{(1,1)} & sb_{(1,2)} & sb_{(1,3)} & sb_{(1,4)} & sb_{(1,5)} & sb_{(1,6)} \\ sb_{(2,1)} & sb_{(2,2)} & sb_{(2,3)} & sb_{(2,4)} & sb_{(2,5)} & sb_{(2,6)} \\ sb_{(1',1)} & sb_{(1',2)} & sb_{(1',3)} & sb_{(1',4)} & sb_{(1',5)} & sb_{(1',6)} \\ sb_{(2',1)} & sb_{(2',2)} & sb_{(2',3)} & sb_{(2',4)} & sb_{(2',5)} & sb_{(2',6)} \\ . & . & . & . & . & . \\ sb_{(n,1)} & sb_{(n,2)} & sb_{(n,3)} & sb_{(n,4)} & sb_{(n,5)} & sb_{(n,6)} \\ sb_{(m,1)} & sb_{(m,2)} & sb_{(m,3)} & sb_{(m,4)} & sb_{(m,5)} & sb_{(m,6)} \\ sb_{(n',1)} & sb_{(n',2)} & sb_{(n',3)} & sb_{(n',4)} & sb_{(n',5)} & sb_{(n',6)} \\ sb_{(m',1)} & sb_{(m',2)} & sb_{(m',3)} & sb_{(m',4)} & sb_{(m',5)} & sb_{(m',6)} \end{bmatrix} \tag{3}$$

$$ABI = \begin{bmatrix} \Delta\hat{P}_{a(1,1)} & \Delta\hat{P}_{b(1,2)} & \Delta\hat{P}_{c(1,3)} & \Delta\hat{V}_{a(1,1)} & \Delta\hat{V}_{b(1,2)} & \Delta\hat{V}_{c(1,3)} \end{bmatrix}$$

$$\Delta\hat{P}_{(1,j)} = \min \left\| \begin{matrix} \Delta P_{i,j} \\ \Delta\hat{P}_{r,j} \end{matrix} \right\|, \quad \Delta\hat{V}_{(1,k)} = \min \left\| \begin{matrix} \Delta V_{i,k} \\ \Delta\hat{V}_{r,k} \end{matrix} \right\| \tag{4}$$

computational burden, to keep adequate estimation accuracy, and at the same time to comply with the single-simulation workflow requirements of the iTesla toolbox, a new method is required. In the iTesla toolbox, it is possible to configure sequential events (e.g. load perturbations, line trips etc.) to be applied to a single network configuration during each single simulation. Hence, a new method that uses sequential events and complies with the workflow requirements of the iTesla toolbox was developed and is explained in the sequel.

B. ASSUMPTIONS AND REQUIREMENTS

The tool's off-line workflow allows to carry out only one time-domain simulation, from which the resulting data is used as input to the VS severity index calculation. The time-domain simulation consists of one pre-contingency operating condition followed by a minimum of three post-contingency operating conditions as shown in Fig. 2.

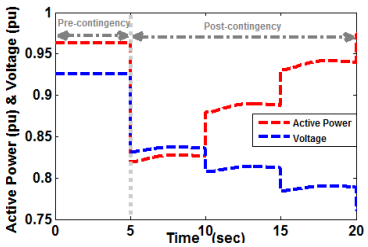

FIGURE 2. Time-domain simulation showing three post-contingency operating conditions.

A minimum of three operating points is required to estimate the PV curve for a given network configuration. In the pre-contingency operating state, only one operating condition from time-domain simulations is necessary as the remaining operational conditions are derived from operational and nameplate data that is available in the platform. Two pre-contingency operating conditions can be derived from the no load operating point (α, β) and an operational point based on the voltage limits $(V_{o\,\mathrm{lim}}, P_1)$ and the MVA limits $(V_2, P_{o\,\mathrm{lim}})$ of the line in pre-contingency state. P_1 is the active power for which the bus voltage reaches the operational voltage limit $V_{o\,\mathrm{lim}}$ for the given bus that can be calculated using power flow. Similarly, V_2 is the voltage of the bus for which active power flow reaches the operational limit $P_{o\,\mathrm{lim}}$ and this can also be calculated using power flow. Using these operating points two PV curves are estimated for the pre-contingency state as shown in Fig. 3. and the "exact" (theoretical solution) PV curve lies between these estimated PV curves.

C. ALGORITHM

Considering the assumptions and required data listed in the previous section, Fig. 4. explains the new algorithm for the VS severity index calculation. The new VS severity

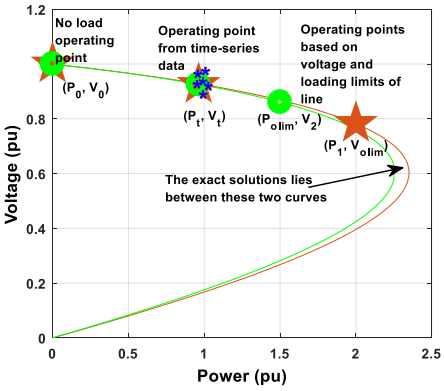

FIGURE 3. Pre-contingency PV curve estimation.

index calculation algorithm is carried out in the following steps.

Step 1. Time-series from time-domain simulations can be divided into one pre- and three post contingency states.
Step 2. Using the post-contingency operation states (P_i, Q_i) from time series data, (α, β) are estimated by solving (1).
Step 3. Using the estimated (α, β) values and $(\bar{V}_i, \bar{P}_i)$ from time series data, the post-contingency PV curve is estimated by solving (2) using least squares.
Step 4. Time series $(\bar{V}_1, \bar{P}_1, \bar{Q}_1)$ and the input values that correspond to the no load operating point (V_0, P_0), voltage limits $(V_{o\,\mathrm{lim}}, P_1)$ and MVA limits $(V_2, P_{o\,\mathrm{lim}})$ of the line; the pre-contingency PV curve can be solved (2) using least squares.
Step 5. Using the estimated PV curves and input operation states, the severity indexes are calculated as explained in Section-2.

D. DATA SYNTHESIS

The added value of the new method and index computation approach in synthesizing information is quantified by the data synthesis factor defined next. This factor allows to quantify the need of storage by aggregating the information contained in the time series. As shown in the following section, it is important to note that the indexes preserve the most important from the time series. The data synthesis factor is given by,

$$\frac{XXkB(data)}{XXkB(indexes)} = y\,fold \tag{6}$$

Where XXkB(data) is the memory used by the raw time-series data and XXkB(indexes) is the memory used by the indexes.

E. SUMMARY OF ADVANTAGES OF THE

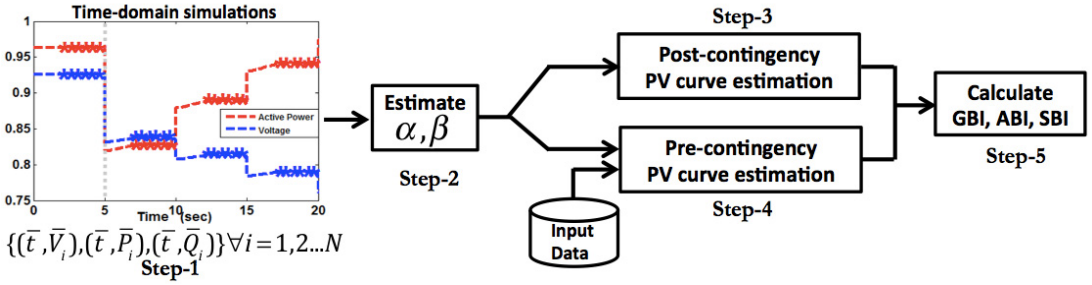

FIGURE 4. Index computation flow chart.

PROPOSED METHOD

The proposed method requires only one time-domain simulation per contingency, and the accuracy of the margin's estimation is maintained by introducing load perturbations to identify the slow-voltage dynamic characteristics of the system.

IV. COMPUTATIONAL AND ACCURACY ANALYSIS

A. ILLUSTRATIVE EXAMPLE

This section illustrates the use of the proposed algorithm for index computations as described in the above sections and the interpretation of its results. The aim is to calculate the distance from different operating points in pre-and-post contingency states to the maximum operational limits in terms of voltage and power. For this illustrative example, a simple two-bus system connected with two lines shown in Fig. 1. is used. A time-domain simulation was carried out for 20 seconds. A contingency was applied at the 5th sec and sequential load perturbations were applied every five seconds after the contingency until the end of the simulation. The time-domain simulation with voltage and power along the time axis is shown in Fig. 5. and the estimated post-contingency PV curve is shown in Fig. 6.

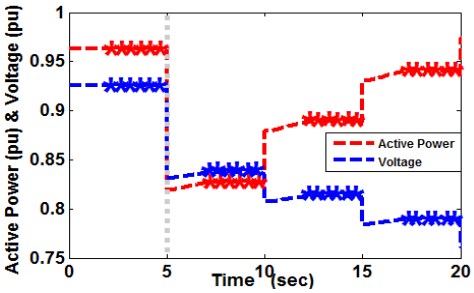

FIGURE 5. Set of simulations and data required to calculate the index (Base MVA = 100 MVA, Base kV = 400 kV).

Fig. 7. depicts the estimated post contingency curve with respect to estimated pre-contingency curves. These curves were estimated using the blue and red data points highlighted in Fig. 5. which are shown as brown circles on the pre-contingency curve and red color (small) circles on the post-contingency curve. It can be observed from Fig. 7. that

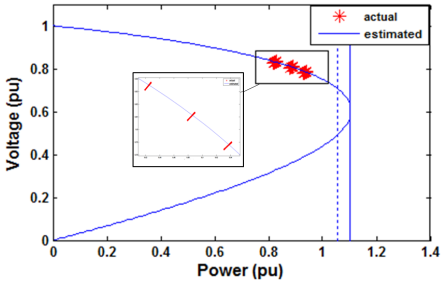

FIGURE 6. Estimated post-contingency PV curve.

the post-contingency curve (red) is smaller than the pre-contingency curves (blue, green) because the impedance of the system increased after the disturbance in the network at the 5th sec. It should also be noted that the distances ($\Delta P's$ and $\Delta V's$) in the post-contingency are smaller than in pre-contingency and negative in some cases. In post-contingency, the curve shrinks and the power transfer limit decreases.

TABLE 1. Voltage stability indexes for the synthetic 2-bus power system.

GBI				$\Delta\bar{P}$	$\Delta\bar{V}$		
				-0. 89	**-0.03**		
ABI		$\Delta\hat{P}_a$	$\Delta\hat{P}_b$	$\Delta\hat{P}_c$	$\Delta\hat{V}_a$	$\Delta\hat{V}_b$	$\Delta\hat{V}_c$
			0.09	**-0.89**	0.49	0.15	**-0.03**
		ΔP_a	ΔP_b	ΔP_c	ΔV_a	ΔV_b	ΔV_c
SBI	B_{11}	1.00	0.55	0.30	0.52	0.41	0.31
	$\hat{B}_{11}$	1.00	0.09	-0.42	0.49	0.15	-0.03
	B_{12}	1.00	0.57	0.11	0.57	0.45	0.23
	$\hat{B}_{12}$	1.00	0.09	**-0.89**	0.49	0.15	**-0.03**

After estimating the equivalent model, the algorithm is applied, and the obtained results are given in TABLE 1. The GBI is used to interpret the given operating point that is very near to the voltage stability limits of the system. In this case, both the elements of the GBI are negative indicating that at least a power and voltage limit was violated. The ABI is used to retrieve more specific information i.e. in this case elements (1, 3) and (1, 6) of the given load levels are negative indicating

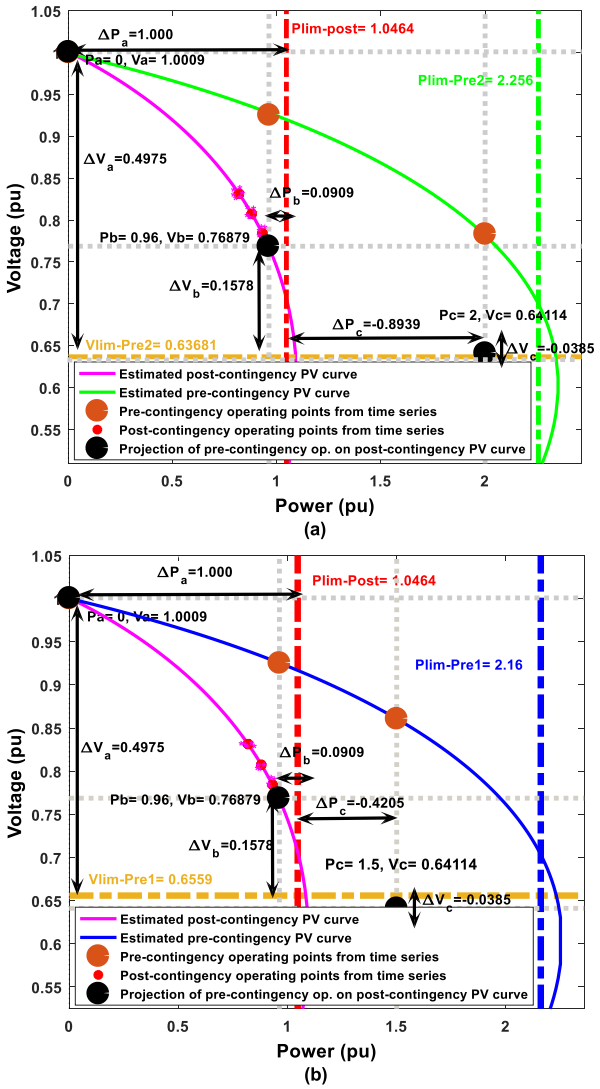

FIGURE 7. Estimated PV curves using pre-and-post-fault data, distance to power and voltage limits. (a) Post-contingency w.r.t pre-contingency curve one. (b) Post-contingency w.r.t pre-contingency curve one.

that there are violations at heavy loading level in both power and voltage.

From the SBI it can be observed that elements (4, 3) and (4, 6) are negative, indicating that during post-contingency these loading levels are on the right-hand side of the power limit and below the voltage limit as shown in Fig. 7(a) and 7(b). Thus, from the severity index it can be interpreted that operation of the system at this loading level will lead voltage instability for the applied disturbance.

B. COMPUTATIONAL BENEFITS AND ACCURACY COMPARISONS

The voltage stability indexes calculated using the previous method from [24] is given in TABLE 2.

From the results given in Table 1 and 2, it can be observed that the calculated indexes using both methods are quantitatively comparable. The new method was developed such that

TABLE 2. Voltage stability indexes computed using [24].

GBI			$\Delta\overline{P}$	$\Delta\overline{V}$		
			-0.78	**-0.03**		
ABI	$\Delta\hat{P}_a$	$\Delta\hat{P}_b$	$\Delta\hat{P}_c$	$\Delta\hat{V}_a$	$\Delta\hat{V}_b$	$\Delta\hat{V}_c$
	1.00	-0.42	**-0.78**	0.49	-0.03	**-0.03**
SBI	ΔP_a	ΔP_b	ΔP_c	ΔV_a	ΔV_b	ΔV_c
	1.00	0.31	0.09	0.53	0.32	0.21
	1.00	-0.42	**-0.78**	0.49	-0.03	**-0.03**

it estimates two pre-contingency PV curves between which the "exact" solution of the PV curve exists. For example, the voltage stability index for the third operating point in the new method (in IV-B) is negative, which implies that the given operating point violates voltage stability limits during post-contingency. The same can be observed from the indexes (in TABLE 2) calculated using old method. The data synthesis factor for both the methods is calculated and tabulated below.

TABLE 3. Data synthesis factor.

Method	Data (kB)	Indexes (kB)	Data synthesis factor
Old	42	0.160	262.50
New	23	0.256	89.843

It can be observed from IV-C that the new method requires less data (time-series) and preserves more information (index, pre-contingency) while at the same time achieves higher reduction. This will be further described in the following section for a larger network and time-series data set where this becomes more obvious. The new method not only reduces them from $O(3n)$ to $O(n)$ (where n is the number of time-domain simulations to be executed), but also provides good estimates of the margin. It can be observed from Fig. 8. that as the number of calculations is increased, a runtime burden on $O(3n)$ (old method) is higher than $O(n)$ (proposed method). Thus, making the proposed method computational more efficient than the previous one.

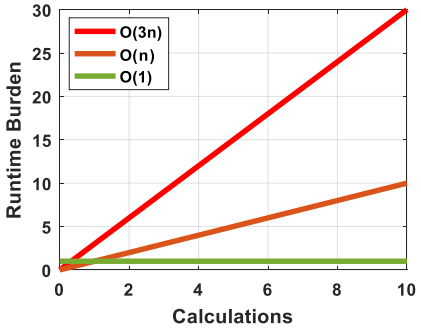

FIGURE 8. Comparisons of runtime characterstics of $O(3n)$ (old method) and $O(n)$ (proposed method).

For the sake of completeness, a CPF routine [25] is also executed on the given network in order to cross-validate the

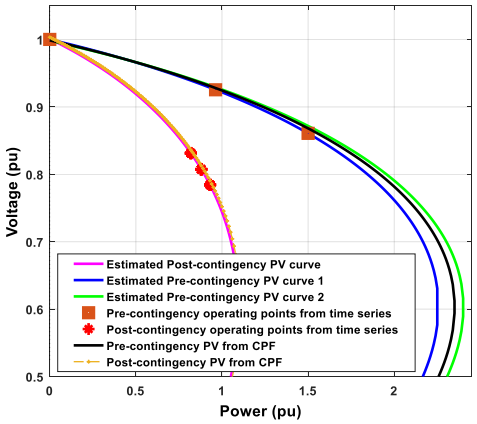

FIGURE 9. Estimated PV curves vs PV curves from a CPF.

PV curves estimated by the new method. It can be observed from Fig. 9. that the estimated post-contingency PV curve exactly matches with the PV curve estimated by CPF routine.

The pre-contingency PV curve from CPF routine lies between the estimated pre-contingency PV curves as explained earlier that the exact PV curve lies between the estimated PV curves in this new method.

C. PERFORMANCE OF THE PROPOSED METHOD WITH DIFFERENT TYPES OF LOAD AND A cpf ALGORITHM

The proposed method is tested with the following types of loads using the IEEE 14 bus system as a network:

- Voltage Dependent Load
- ZIP load
- Frequency Load
- Thermostatically Controlled Load

The details of the above load models are available in [26]. The estimated PV curves for the above load models are shown in Fig. 10. The new method was developed such that it estimates the region (two pre-contingency PV curves) where the "exact" solution of the PV curve exists. It can be observed from the figures that the PV curve from CPF lies between the estimated PV curves. It can also be observed from Fig. 10. that the method performs well for the given type of loads because the CPF solution is always in the estimated region (between the estimated PV curves).

This method is also tested with a PQ load connected to the secondary side of Under Load Tap Changer (ULTC) and the details of the ULTC model are available in [26]. In this case, the primary side voltages of the ULTC are used to estimate the region of the PV curve. The estimated PV curves along with the CPF solution are shown in Fig. 11. It can be observed that actual PV curve is in the region estimated by the proposed method (between the estimated PV curves).

V. APPLICATION TO THE NORDIC-44 BUS SYSTEM

In this section the proposed index is tested on using simulation time-series from the Nordic-44 bus system. First the

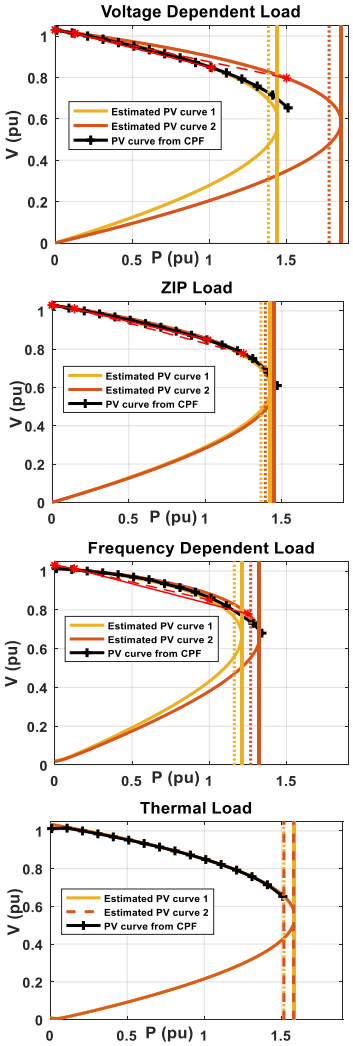

FIGURE 10. Estimated PV curves for different types of loads.

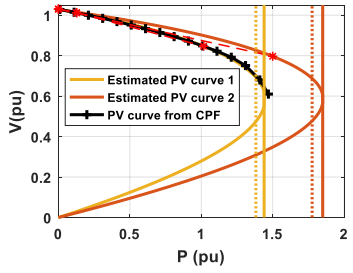

FIGURE 11. Estimated PV curve with ULTC.

system is described; later different case studies and analyses of the obtained results are presented.

A. SYSTEM DESCRIPTION

The Nordic-44 Bus test system is an equivalent representation of the Nordic grid (Sweden, Norway and Finland) as shown in Fig. 12. and was originally implemented in PSS/E [21], [22]. It consists of 44 buses, 61 generators with

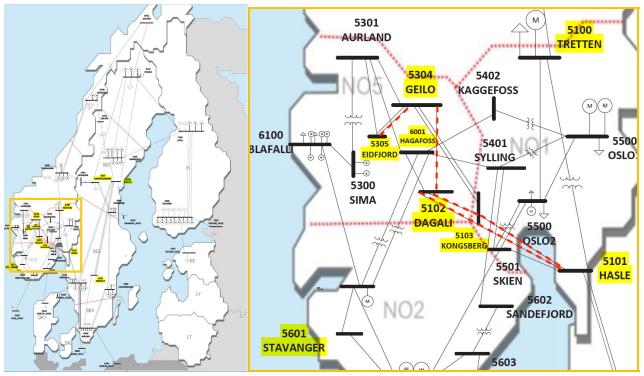

FIGURE 12. Nordic-44 power system model and the fault area used in the case studies.

various control systems (exciter, turbine, governor and stabilizer), 67 transmission lines (420 kV and 300 kV) and 43 loads. The regions shown in this model are defined according to the Nordic electricity market bidding regions. The historical market data was matched w.r.t the power flow results for this model and the details can be found in [22].

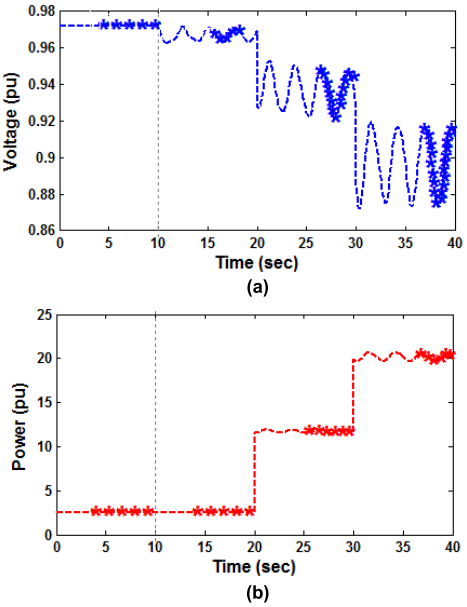

FIGURE 13. Set of simulations and data required to calculate the index. (a) Voltage at Bus 5304. (b) Power at Bus 5304.

B. CASE STUDY-1-SINGLE LINE TRIP

In this case study, one of the double circuit lines between Bus 5304 and 5305 in the NO5 region in Norway was tripped at 10^{th} sec (red dotted line to the farthest left in the zoom-in box). Load perturbations are applied every 10 seconds after the contingency until the end of the simulation. The load perturbations are selected such that it covers low, acceptable and high loading levels. The voltage and power at Bus 5304 are shown in Fig. 13. An initial load of 250 MW was considered and is increased at the end of the 20^{th} and 30^{th} sec

TABLE 4. Voltage stability indexes for case study 1.

GBI				$\Delta\bar{P}$	$\Delta\bar{V}$		
				0.22	**0.32**		
ABI		$\Delta\hat{P}_a$	$\Delta\hat{P}_b$	$\Delta\hat{P}_c$	$\Delta\hat{V}_a$	$\Delta\hat{V}_b$	$\Delta\hat{V}_c$
		1.00	0.93	**0.22**	0.58	0.5729	**0.3223**
		ΔP_a	ΔP_b	ΔP_c	ΔV_a	ΔV_b	ΔV_c
SBI	B_{11}	1.00	0.94	0.52	0.59	0.57	0.46
	$\hat{B}_{11}$	1.00	0.93	0.43	0.58	0.57	0.42
	B_{12}	1.00	0.94	0.29	0.59	0.57	0.36
	$\hat{B}_{12}$	1.00	0.93	**0.22**	0.58	0.57	**0.32**

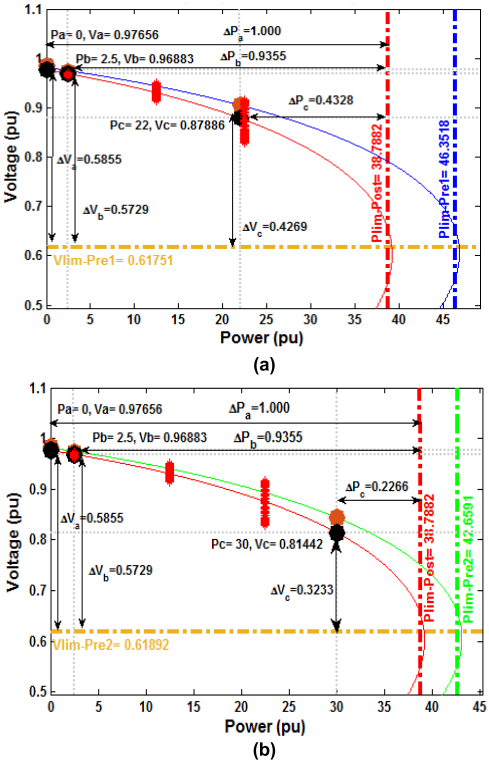

FIGURE 14. Estimated PV curves using pre-and-post-fault data, distance to power and voltage limits. (a) Post-contingency w.r.t pre-contingency curve-1. (b) Post-contingency w.r.t pre-contingency curve-2.

as shown in Fig. 13(b). It can also be observed in Fig. 13(a) that the voltage at the bus drops after the contingency and it further decreases with an increase in load power consumption. Voltage and active power values at the no load operating condition, minimum voltage limit operating condition and maximum loading limit operating condition are given as an input for estimating pre-contingency PV curves. Using the pre-and-post contingency data and other platform data the proposed voltage stability index was calculated using signals from bus Geilo (Bus No. 5304). The obtained results are given in TABLE 4 and the post contingency PV curves w.r.t both pre-contingency curves are shown in Fig. 14. In this case study, the limits are set to 10% less than the theoretical limits ($\varepsilon = 0.1$).

TABLE 5. Voltage stability indexes for case study 2.

		Line trip C1						Line trip C2						Line trip C3						Line trip C4					
GBI				**-0,14**			**-0,01**			**-0,26**			**-0,01**			**-0,20**			**-0,01**			0,01			0,09
ABI		1,0	0,91	**-0,14**	0,59	0,57	**-0,01**	1,0	0,92	**-0,26**	0,59	0,57	**-0,01**	1,0	0,92	**-0,20**	0,59	0,57	**-0,01**	1,0	0,93	0,01	0,59	0,58	0,09
SBI	B_{5102}	1,0	0,94	0,48	0,60	0,58	0,45	1,0	0,94	0,48	0,59	0,57	0,45	1,0	0,94	0,48	0,60	0,58	0,46	1,0	0,94	0,48	0,59	0,57	0,45
	$\hat{B}_{5102}$	1,0	0,91	0,18	0,59	0,57	0,29	1,0	0,94	0,42	0,60	0,59	0,43	1,0	0,93	0,38	0,59	0,58	0,41	1,0	0,94	0,47	0,59	0,58	0,44
	$B_{5102'}$	1,0	0,94	0,30	0,59	0,57	0,37	1,0	0,95	0,30	0,59	0,58	0,37	1,0	0,95	0,30	0,59	0,57	0,37	1,0	0,95	0,30	0,59	0,58	0,37
	$\hat{B}_{5102'}$	1,0	0,91	**-0,14**	0,59	0,57	**-0,01**	1,0	0,94	0,19	0,60	0,59	0,31	1,0	0,93	0,14	0,59	0,58	0,26	1,0	0,94	0,26	0,59	0,58	0,35
	B_{5103}	1,0	0,95	0,54	0,59	0,58	0,47	1,0	0,95	0,54	0,59	0,58	0,47	1,0	0,95	0,54	0,59	0,58	0,47	1,0	0,95	0,54	0,59	0,58	0,47
	$\hat{B}_{5103}$	1,0	0,93	0,29	0,59	0,57	0,36	1,0	0,92	0,16	0,59	0,57	0,28	1,0	0,92	0,20	0,59	0,57	0,31	1,0	0,93	0,34	0,59	0,58	0,39
	$B_{5103'}$	1,0	0,96	0,33	0,60	0,59	0,39	1,0	0,96	0,33	0,61	0,59	0,39	1,0	0,96	0,33	0,59	0,58	0,38	1,0	0,96	0,33	0,59	0,58	0,38
	$\hat{B}_{5103'}$	1,0	0,93	**-0,07**	0,59	0,57	**-0,01**	1,0	0,92	**-0,26**	0,59	0,57	**-0,01**	1,0	0,92	**-0,20**	0,59	0,57	**-0,01**	1,0	0,93	0,01	0,59	0,58	0,09
	B_{5304}	1,0	0,95	0,53	0,60	0,58	0,47	1,0	0,95	0,53	0,60	0,58	0,47	1,0	0,95	0,53	0,60	0,58	0,47	1,0	0,95	0,53	0,60	0,58	0,47
	$\hat{B}_{5304}$	1,0	0,94	0,46	0,59	0,58	0,44	1,0	0,94	0,45	0,59	0,57	0,44	1,0	0,94	0,49	0,59	0,57	0,45	1,0	0,94	0,47	0,60	0,57	0,46
	$B_{5304'}$	1,0	0,94	0,30	0,59	0,57	0,37	1,0	0,94	0,30	0,59	0,57	0,37	1,0	0,94	0,31	0,59	0,58	0,37	1,0	0,94	0,30	0,59	0,57	0,37
	$\hat{B}_{5304}$	1,0	0,94	0,27	0,59	0,57	0,35	1,0	0,94	0,26	0,59	0,57	0,34	1,0	0,94	0,30	0,59	0,57	0,37	1,0	0,94	0,28	0,60	0,56	0,37

TABLE 6. Data synthesis factor for case study 2.

Contingency	Old Method			New Method		
	Data (kB)	Indexes (kB)	Data synthesis factor	Data (kB)	Indexes (kB)	Data synthesis factor
C1,C2,C3,C4	120	0.352	340.90	81	0.64	126.56

These curves are estimated using the data highlighted in blue and red colour in Fig. 13. and these points are plotted in brown colour on the pre-contingency curve (blue, green) and in red colour points on the post-contingency curve (red) as shown in Fig. 14.

DISCUSSION OF THE RESULTS IN CASE STUDY 1

It can be observed from TABLE 4 that both the elements of GBI are close to zero and non-negative. This indicates that the voltage and power limits are not violated. The same can be observed in Fig. 14. On further inspection of the SBI it is found that the loading level on bus 5304 has a narrow margin to the limits in post-contingency. Thus, from the severity index it can be interpreted that although the operation of the system at this loading level is not violating the power and voltage limits of the system, if this loading is reached after the occurrence of this contingency, then the operational margin is significantly low. This relative measure of strength of the contingency can be used in dynamic analysis tools [27] or in developing preventive control actions based on machine learning techniques [28].

C. CASE STUDY-2-MULTIPLE LINE TRIPS

In this case study, four contingencies are created and analyzed. The lines between the buses 5101-5102, 5101-5103, 5102-5103 and 5103-5304 are tripped and are labeled as C1, C2, C3 and C4, respectively. VS severity index was calculated with respect to three buses (buses 5102, 5103, and 5304) for each of the above-mentioned contingencies. Twelve simulations were performed in total as shown in TABLE 5. At the end of simulation twelve PV curves are obtained (omitted due to space limitations). The operational limits used to compute the index were set to 10% less than the theoretical limits ($\varepsilon = 0.1$) for both powers and voltages.

DISCUSSION OF THE RESULTS IN CASE STUDY 2

Even though the PV curves and simulation results are not shown herein due to space limitations, the indexes presented in TABLE 5 provide sufficient synthetic information for analysis. It can be observed from the GBI results that out of the four contingencies analyzed, only in C1, C2 and C3 there are violations of power and voltage limits. It can also be observed from the ABI that for all contingencies the power and voltage violation occurred at heavy loading conditions. A close look at the SBI results indicates that for contingency C1 two buses violated power and voltage limits signifying the importance of the line with respect to voltage stability. The indexes plotted in Fig. 15. shows that bus 5103 violates voltage stability limits in the post-contingency for the contingencies C1, C2 and C3. This indicates that bus 5103 is most

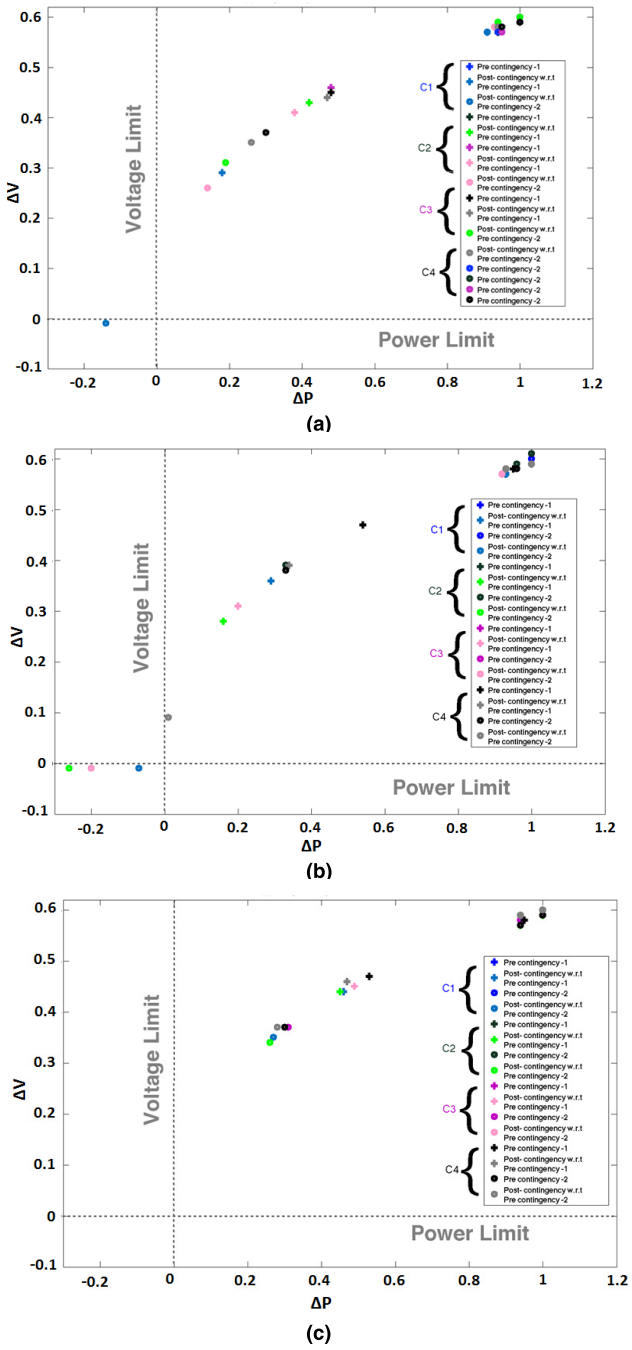

FIGURE 15. Calculated voltage stability indexes for buses (a) 5102 (b) 5103 and (c) 5304. (a) Voltage Stability indexes for bus 5102. (b) Voltage Stability indexes for bus 5103. (c) Voltage Stability indexes for bus 5304.

sensitive to the events C1, C2 and C3. The index also shows that contingency C4 is the least significant when compared to all the contingencies in the study.

It can be observed from TABLE 6 that the new method requires less time-series data and it preserves more information while at the same time achieving higher reduction. The same can be observed and interpreted from the calculated data synthesis factor.

VI. CONCLUSION

In this paper, a new methodology to compute a modified three-layer severity index to assess power system voltage stability was described. Unlike the previous index computation approach [24], which requires $O(3n)$ time-domain simulations, the new algorithm requires only one time domain simulation per contingency with sequential load perturbations $O(n)$ to calculate the severity of the contingency. The method replaces the requirement of running multiple simulations by extracting equivalent knowledge from the DSA platform's input data on no load voltage conditions. These modifications were made in order to comply with the software architecture of the iTesla platform, however, it can be readily used by other DSA tools, especially those without dedicated CPF routine. The data synthesis factor is calculated to highlight the value of the new method in synthesizing the information. Future work will focus on the deployment of this new approach on a platform that will use it to generate voltage stability rules via machine-learning techniques.

REFERENCES

[1] K. Moslehi and R. Kumar, "A reliability perspective of the smart grid," *IEEE Trans. Smart Grid*, vol. 1, no. 1, pp. 57–64, Jun. 2010.

[2] C. Vournas and T. Van Cutsem, "Online voltage stability assessment," in *Real-Time Stability in Power Systems*, 2nd ed. New York, NY, USA: Springer, 2014, ch. 10, pp. 305–333.

[3] Y. Sun, P. Wang, L. Cheng, and H. Liu, "Operational reliability assessment of power systems considering condition-dependent failure rate," *IET Gener., Transmiss. Distrib.*, vol. 4, no. 1, pp. 60–72, Jan. 2010.

[4] G. K. Morison, B. Gao, and P. Kundur, "Voltage stability analysis using static and dynamic approaches," *IEEE Trans. Power Syst.*, vol. 8, no. 3, pp. 1159–1171, Aug. 1993.

[5] Y.-H. Moon, H.-S. Ryu, J.-G. Lee, and B. Kim, "Uniqueness of static voltage stability analysis in power systems," in *Proc. Power Eng. Soc. Summer Meeting*, Jul. 2001, pp. 1536–1541.

[6] H.-D. Chang, C.-S. Wang, and A. J. Flueck, "Look-ahead voltage and load margin contingency selection functions for large-scale power systems," *IEEE Trans. Power Syst.*, vol. 12, no. 1, pp. 173–180, Feb. 1997.

[7] K. Morison, H. Hamadanizadeh, and L. Wang, "Dynamic security assessment tools," in *Proc. IEEE Power Eng. Soc. Summer Meeting*, Edmonton, AB, Canada, Jul. 1999, pp. 282–286.

[8] A. Bihain *et al.*, "OMASES: A dynamic security assessment tool for the new market environment," presented at the IEEE Bologna Power Tech Conf., Jun. 2003.

[9] S. Massucco and M. Pavella, "OMASES-open market access and security assessment system: An approach to preventive dynamic security assessment and control," in *Proc. IEEE Power Eng. Soc. Summer Meeting*, vol. 3, Jul. 2002, pp. 1407–1409.

[10] J. Tong and L. Wang, "Design of a DSA tool for real time system operations," presented at the Int. Conf. Power Syst. Technol., Chongqing, China, 2006.

[11] R. Avila-Rosales, J. Giri, and R. Lopez, "Extending EMS capabilities to include online stability assessment," in *Proc. IEEE PES Power Syst. Conf. Expo. (PSCE)*, New York, NY, USA, Oct. 2004, pp. 1671–1675, Paper 04PS0371.

[12] L. Loud *et al.*, "Hydro-Québec's challenges and experiences in online DSA applications," presented at the IEEE PES Gen. Meeting, Minneapolis, MI, USA, Jul. 2010.

[13] U. Kerin, R. Balaurescu, F. Lazar, R. Krebs, and F. Balasiu, "Dynamic security assessment in system operation and planning—First experiences," in *Proc. IEEE Power Energy Soc. Gen. Meeting*, Jul. 2012, pp. 1–6.

[14] J.-Y. Astic *et al.*, "Control center designs: New functions and challenges for the transmission system operator," *IEEE Power Energy Mag.*, vol. 16, no. 2, pp. 57–66, Mar./Apr. 2018.

[15] M. H. Vasconcelos *et al.*, "Online security assessment with load and renewable generation uncertainty: The iTesla project approach," in *Proc. Int. Conf. Probalistic Methods Appl. Power Syst. (PMAPS)*, Beijing, China, Oct. 2016, pp. 1–8.

[16] I. Konstantelos *et al.*, "Implementation of a massively parallel dynamic security assessment platform for large-scale grids," *IEEE Trans. Smart Grid*, vol. 8, no. 3, pp. 1417–1426, May 2016.
[17] V. S. N. Arava and L. Vanfretti, "Analyzing the static security functions of a power system dynamic security assessment toolbox," *Int. J. Elect. Power Energy Syst.*, vol. 101, pp. 323–330, Oct. 2018, doi: 10.1016/j.ijepes.2018.03.033.
[18] S. Massucco, S. Grillo, A. Pitto, and F. Silvestro, "Evaluation of some indices for voltage stability assessment," in *Proc. IEEE Power Tech Conf.*, Bucharest, Romania, Jul. 2009, pp. 1–8.
[19] C. A. Canizares, A. C. Z. D. Souza, and V. H. Quintana, "Comparison of performance indices for detection of proximity to voltage collapse," *IEEE Trans. Power Syst.*, vol. 11, no. 3, pp. 1441–1450, Aug. 1996.
[20] S. C. Savulescu, *Real-Time Stability Assessment in Modern Power System Control Centers*. Hoboken, NJ, USA: Wiley, 2009.
[21] L. Vanfretti, T. Rabuzin, M. Baudette, and M. Murad, "iTesla power systems library (iPSL): A modelica library for phasor time-domain simulations," *Softw. X*, vol. 5, pp. 84–88, May 2016, doi: 10.1016/j.softx.2016.05.001.
[22] L. Vanfretti *et al.*, "An open data repository and a data processing software toolset of an equivalent nordic grid model matched to historical electricity market data," *Data Brief*, vol. 11, pp. 349–357, Apr. 2017, doi: 10.1016/j.dib.2017.02.021.
[23] M. Parniani, J. Chow, L. Vanfretti, B. Bhargava, and A. Salazar, "Voltage stability analysis of a multiple-infeed load center using phasor measurement data," in *Proc. IEEE PES Power Syst. Conf. Expo. (PSCE)*, Oct./Nov. 2006, pp. 1299–1305.
[24] L. Vanfretti and F. R. S. Sevilla, "A three-layer severity index for power system voltage stability assessment using time-series from dynamic simulations," in *Proc. IEEE PES Innov. Smart Grid Technol. Eur. (ISGT)*, Oct. 2014, pp. 1–5.
[25] F. Milano, "Continuation power flow analysis," in *Power System Modelling and Scripting*. New York, NY, USA: Springer, 2010.
[26] F. Milano, *PSAT, Version 2.1.8*, document, Jan. 2013.
[27] N. Samaan *et al.*, "Dynamic contingency analysis tool—Phase 1," Pacific Northwest Nat. Lab., Richland, WA, USA, Tech. Rep. PNNL-24843, Nov. 2015.
[28] C. Liu *et al.*, "A systematic approach for dynamic security assessment and the corresponding preventive control scheme based on decision trees," *IEEE Trans. Power Syst.*, vol. 29, no. 2, pp. 717–730, Mar. 2014.

V. S. NARASIMHAM ARAVA (M'17) received the B.Tech. degree in electrical and electronics engineering from Acharya Nagarjuna University, India, in 2011, and the M.Sc. degree in electric power engineering from the KTH Royal Institute of Technology, Stockholm, Sweden, in 2016. He was a Power System Studies Engineer with Power Research and Development Consultants (PRDC) Private Limited, India, from 2011 to 2014, and was a Research Engineer with the SmarTS Lab, KTH Royal Institute of Technology, from 2016 to 2017. He is currently a Power System Engineer with WAMS Center of Excellence, GE, Edinburgh, U.K. His research interests include a wide range of topics related to power systems modeling, operation and control, and synchrophasor applications with the focus on commercial application of innovative technologies.

LUIGI VANFRETTI (SM'14) received the M.Sc. and Ph.D. degrees in electric power engineering from the Rensselaer Polytechnic Institute, Troy, NY, USA, in 2007 and 2009, respectively. He was with the KTH Royal Institute of Technology, Stockholm, Sweden, as an Assistant, from 2010 to 2013, and an Associate Professor (Tenured) and a Docent from 2013 to 2017, where he led the SmarTS Lab and research group. From 2011 to 2012, he was a consultant with Statnett SF, the Norwegian electric power transmission system operator, where he was a Special Advisor in research and development from 2013 to 2016. He joined the Rensselaer Polytechnic Institute in 2017, where he is currently a Tenured Associate Professor. His research interests are in the areas of synchrophasor technology applications and cyber-physical power system modeling & simulation.